scientific reports

Check for updates

OPEN

Early-Stage degradation of electrolytic iron particle-based magnetorheological elastomer under natural weathering conditions

Rehnupreya Hentry Viension[1], Nur Azmah Nordin[1,2]✉, Saiful Amri Mazlan[1,2], Mohd Aidy Faizal Johari[1], Norman M. Wereley[3], Abdul Yasser Abd Fatah[4], Nursyafiqah Zaini[1] & Michal Sedlacik[5]✉

Magnetorheological elastomer (MRE) is a smart composite possessing properties that can be tuned by an external magnetic field, making them highly attractive for vibration isolation applications. Their reliable use in outdoor environments, however, requires a clear understanding of how natural weathering influences their performance and durability. While most previous research has addressed long-term or accelerated ageing conditions, the onset of environmental degradation of MRE remains insufficiently explored. Therefore, this study investigated the early-stage degradation of MRE, embedded with irregular electrolytic iron particles (MRE-EIP) over six weeks of natural weathering exposure. Weekly samples (W0-W6) were analysed using vibrating sample magnetometer (VSM), rheometer and low vacuum scanning electron microscope and the results were correlated with weathering data from the Malaysian Meteorological Department, Kuala Lumpur. The saturation magnetization, M_s finding shows minimal change from 111.63 Am^2/kg in W0 to 113.79 Am^2/kg in W6, likely attributed to the exposure of EIP following the removal of the aged localized surface over the six week exposure. Strain sweep results meanwhile, revealed the progressive stiffening, with the storage modulus (G') increased from 0.22 MPa (W0) to 0.53 MPa (W6), accompanied by a narrowing linear viscoelastic (LVE) region, indicative of early embrittlement of the samples. Nevertheless, a temporary reduction in G' for W3 suggested a moisture-induced plasticisation, from increased rainfalls that week. Besides, the absolute MR effect, $\Delta G'$ increased from 0.23 MPa (W0) to 0.34 MPa (W6), indicating greater responsiveness of exposed EIP to the magnetic fields which enhanced the G' accordingly. Morphological analysis confirmed the development of localized surface depressions suggests combine effects of UV-driven embrittlement and moisture plasticisation from rainfall, leading to localised EIP exposure, while the cross-sectional structure integrity remained intact. These findings provide the first detailed account of early-stage degradation in MRE-EIP under natural weathering, offering valuable insights into early failure mechanisms and guiding durability driven material design for outdoor smart material applications.

Keywords Magnetorheological elastomer, Electrolytic iron particles, Storage modulus, Magnetorheological effect, UV radiation, Rainfall, Surface degradation

[1]Engineering Materials & Structures (eMast) Ikohza, Malaysia-Japan International Institute of Technology (MJIIT), Universiti Teknologi Malaysia, Kuala Lumpur 54100, Malaysia. [2]Automotive Development Centre, Institute for Sustainable Transport (IST), Universiti Teknologi Malaysia, Skudai 81310, Johor, Malaysia. [3]Composites Research Laboratory, University of Maryland, College Park, Maryland 20742, USA. [4]Department of Smart Engineering and Advanced Technology (SEAT), Faculty of Artificial Intelligence (FAI), Universiti Teknologi Malaysia, Kuala Lumpur 54100, Malaysia. [5]Department of Production Engineering, Faculty of Technology, Tomas Bata University in Zlín, Zlín 760 01, Czech Republic. ✉email: nurazmah.nordin@utm.my; msedlacik@utb.cz

Magnetorheological elastomer (MRE) is a smart composite comprised of rubber matrix embedded with soft magnetic particles, particularly iron particles. The unique property of MRE lies in their capability to alter their mechanical characteristics when subjected to an external magnetic field, a response that has been facilitated by the interactions of magnetic particles within the elastomeric matrix towards the magnetic field[1]. Such magnetic field-dependent behavior allows MRE to undergo rapid and reversible changes through controlled variation of magnetic flux density, enabling their use in a wide range of smart engineering applications. This tunability under external stimuli is especially valuable in areas requiring real-time adaptability, such as in civil infrastructure like vibration or base isolators[2,3] in buildings and bridges, where dynamic control of stiffness and damping can enhance performance and safety.

As MRE hold promises for a wide range of applications with distinct functional and structural requirements, ongoing research is dedicated to developing and tailoring these materials to meet diverse performance demands. In recent years, various efforts have been made to alter and enhance the properties of MRE such as by incorporating different additives[4,5], optimizing volume fractions of magnetic particles[6,7], refining the alignment of magnetic particles at specific angles[8,9], and utilizing different matrix materials[10,11]. While building on research focuses on the magnetic particles in the matrices, researchers have begun studying the impact of different shapes of iron particles in enhancing the properties of MRE. In particular, irregular electrolytic iron particles (EIP) are gaining attention due to their ability to strengthen the interaction between magnetic particles and the matrix material, making it a promising approach to improve the properties of MRE. While spherical carbonyl iron particles (CIP) are well known and commonly use in MRE due to high magnetic saturation (M_s), excellent permeability, and low resistance to magnetization (coercivity)[12], EIP also offers distinct advantages that render it becomes a compelling alternative to CIP in the fabrication of MRE.

Several studies have reported that the mechanical and magnetorheological (MR) properties of MRE could be enhanced when EIP were used as the filler. For instance, Kumar et al.[13] demonstrated the increased in elastic modulus by approximately 13% and load-bearing capacity by about 40% for MRE-EIP, compared to the MRE-CIP. These improvements might be due to more efficient stress transfer from the polymer chains to the EIP flocs under the increasing strains, which allows for better load distribution across the matrix and reduces localized deformation. Similarly, Alam et al.[14] confirmed that the MRE containing EIP as filler exhibited higher load-bearing capacities than those of MRE with CIP, further highlighting the superiority of EIP as a reinforcing agent. This was primarily attributed to the irregular and uneven surface of EIP, which allowed for better interlocking and integration of particles within the elastomer network. As a result, the MR effect of the material was found to be 9% higher, indicating the enhanced particle-matrix interaction facilitated by the EIP's rough surface texture. In terms of viscoelastic performance, the MRE-EIP showed an 11% higher in stress relaxation rate under a magnetic field as compared to the MRE-CIP[14]. This improvement is again linked to the superior stress transfer capability by the MRE-EIP, which offer considerable advantages in applications requiring effective damping performance. Faster stress relaxation enables the material to rapidly dissipate mechanical energy, making it ideal for dynamic systems such as automotive suspensions and vibration absorbers that must continuously adapt to changing operational conditions. Both studies emphasized the irregular shape of EIP that plays a pivotal role in enhancing the stress transfer efficiency and strengthening the particle-matrix interfacial interactions, highlighting a promising direction for the development of modified MRE with enhanced performance characteristics. Supporting the findings, Patel et al.[15] confirmed that the EIP that exhibited greater surface area has promoted better filler dispersion and significantly increased the crosslink density within matrix phase, compared to MRE-CIP. In addition, the use of EIP has amplified the relative MR effect, with MRE-EIP achieving a remarkable 256% versus MRE-CIP that only reported 73% of MR effect. Further strengthening the body of knowledge, an extended study by Kumar et al.[16] reported an increase in the compressive modulus of MRE-EIP, by 35% relative to the MRE-CIP, and it is consistent with their earlier findings on the elastic modulus analysis[13]. In addition, the incorporation of EIP along with multi-walled carbon nanotubes (MWCNTs) as additives produced a synergistic effect in the MRE, enhancing both mechanical properties and MR response of the material.

Despite their aforementioned advantages, all materials including MRE are inevitably subjected to persistent environmental stressors that can compromise their long-term functionality[17]. Prolong exposure to ultraviolet (UV) radiation, humidity, and temperature fluctuations has been shown to deteriorate the structural and mechanical integrity of various polymer-based materials. For example, environmental ageing studies on rubber modified polypropylene, polyurethane, and styrene-butadiene rubbers have reported reductions in the tensile strength[18], increased brittleness[19] and induced surface cracks[20], typically attributed to several mechanisms such as photo-oxidation and chain scission. While these materials differ chemically from silicone rubber, a commonly used matrix in MRE, such findings highlighted the broader susceptibility of polymeric systems to weathering-induced degradation. In fact, although the performance benefits of MRE-EIP have been emphasized under controlled laboratory conditions, their behavior under natural environmental exposure remains largely unexplored. This research gap is critical, as environmental degradation may interact gently with the embedded iron particles and the interaction is not adequately represented by studies in other elastomeric systems. Previous investigations on MRE containing CIP[21,22] have shown that natural weathering could significantly influence their stability and reliability. After certain durations of environmental ageing, notable changes in the material properties were observed. For instance, the storage modulus, G' of MRE-CIP sample that was exposed to natural weathering for 30 days has shown increment by approximately 10% under the condition of 0 T, and by 3% under the condition of 0.8 T, compared to unaged MRE-CIP samples under the same respective conditions. In fact, the Young's modulus exhibited a substantial increase of 35%, while elongation at break decreased by 20%, indicating a pronounced stiffening effect of the elastomeric matrix of the MRE-CIP. In addition to these mechanical changes, the surface degradation phenomena such as erosion lines and ozone-induced microcracks were also documented[21]. Meanwhile in other studies, extending the natural weathering exposure to 90 days has caused severe surface degradation in MRE-CIP samples, including microcracks and cavities due to ozone

exposure, as confirmed by the microscale analysis[22]. These effects might be attributed to the photo-oxidation processes, highlighting the importance of understanding weathering mechanisms in the design of durable MRE.

While previous studies have significantly contributed to the understanding of MRE-CIP's degradation, most have relied on fixed-point analyses. Although informative, such approaches provide only snapshots of the degradation process. Besides, albeit very limited, those studies have focused on the degradation of MRE-CIP samples over periods ranging from one to three months. Indeed, a study that focused on the degradation of MRE-CIP samples to natural seawater also was conducted[23]. To better capture the early-stage evolution of the degradation, conducting weekly analyses is essential, particularly under natural weathering conditions. Degradation is a time-dependent process, and subtle changes such as surface oxidation, microcrack initiation, or early stiffening of the matrix phase would be developed gradually and non-linearly. This approach is not only enhancing the understanding of degradation process but also allows for more accurate correlations between the environmental exposure and specific chemical, morphological, and rheological changes. Expanding such approach to continuous monitoring could yield a more detailed understanding of the onset and progression of degradation phenomena. Importantly, early-stage degradation is governed by failure mechanisms that differ from those dominating later stages of exposure. At this stage, subtle changes such as initial matrix hardening or plasticisation , early interfacial weakening, and disruption of particle-matrix interactions may not yet produce visible damage but can critically influence the subsequent evolution toward catastrophic failure. Identifying these early degradation signs is essential for preventing premature performance loss in MRE components. Insight into how early failure initiates also enables targeted reformulation of composite systems to extend service life. From an application perspective, understanding early-stage degradation is particularly important for MRE systems that must deliver reliable functionality immediately after deployment.

Therefore, the present work aims to expand the understanding on how environmental factors such as UV radiation, temperature fluctuations, and rainfall affect the early degradation and performance of MRE-EIP samples. By implementing a systematic weekly analysis framework, the research finding would facilitate the continuous monitoring of material's performance, enabling the detection of nuanced changes that may serve as early indicators of deterioration. Such an approach enables early identification of degradation mechanisms that precede catastrophic failure, providing a foundation for durability driven MRE design. By examining the key environmental effects, the investigation is not only complementing the existing research but also offers fresh insights into the practical applications of MRE-EIP in natural environments.

Materials and methodology

Sample preparation

In this study, MRE-EIP samples were prepared using room temperature vulcanization silicone rubber (SR) as the matrix, supplied by Nippon Steel Co., Japan. The MRE-EIP composed of 40 wt.% of SR and 60 wt.% of EIP, supplied from Industrial Metal Powders Pune, India PVT LTD. The EIP has an average particle diameter of 6 µm and a density of 7.86 g/cm^3. The overall preparation process of MRE-EIP samples is illustrated in Fig. 1, and the preparation involved several steps. In order to prepare one sheet of MRE-EIP that required 68 g of molten MRE-EIP mixture, 40.8 g of EIP was added to the 27.2 g of liquid SR. Then, both components were mixed using a mechanical stirrer at 200 rotations per minute, for 20 min at a room temperature of 25 °C until a visually homogeneous mixture was obtained. Next, 2 wt.% of curing agent (NS625B, Nippon Steel) was incorporated and immediately hand-stirred for another 10 s. The curing agent basically acted as a cross-linking agent, facilitating the vulcanization process and forming the elastomeric network of the MRE-EIP samples. The final mixture then was poured into a flat aluminium mould with the dimensions of 150 mm × 150 mm × 1 mm and left to cure at room temperature for 4 h, without the presence of external magnetic field. After curing, the MRE-EIP sheet was demoulded and trimmed to remove any excess material. The sheet was then cut into strips of 25 mm in width and 150 mm in length prior to weathering exposure process. Five strips of MRE-EIP were obtained from one prepared sheet and to acquire seven strips respective to seven exposed weeks of natural weathering, additional sheet was prepared following the similar steps. Out of seven strips, one would be acted as unaged sample (W0) while the other six strips were designated for natural weathering exposure over weekly durations, namely W1, W2, W3, W4, W5 and W6 for week 1, week 2, week 3, week 4, week 5 and week 6, respectively.

Natural weathering exposure process

MRE-EIP samples were exposed to natural weathering from February 20th 2024 until April 1st 2024 at Malaysia-Japan International Institute of Technology, Universiti Teknologi Malaysia (UTM), located in Kuala Lumpur, Malaysia. MRE-EIP samples were hung vertically (90° inclination) within an open exposure cage, ensuring unrestricted airflow and uniform exposure to the natural weathering. For each exposure duration, three replicate

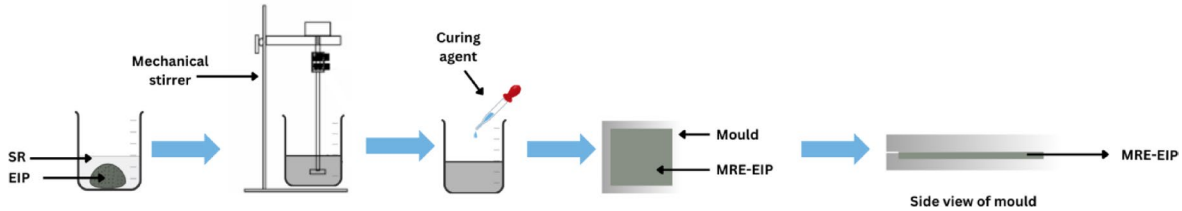

Fig. 1. Preparation of MRE-EIP samples.

samples ($n = 3$) were prepared and subjected to natural weathering under identical conditions. Samples were systematically collected at weekly intervals over the six-week period as stated in previous section. Following each collection, the MRE-EIP samples were cleaned using a lint-free cloth lightly dabbed with acetone. Acetone was selected as the cleaning agent due to its non-reactive nature towards the elastomer and its rapid evaporation, as it is a volatile solvent. After cleaning step, the samples were placed at room temperature inside a desiccator for a minimum of 24 h before the testing process was carried out.

Meanwhile, the weathering data for the exposure period were obtained from the Malaysian Meteorological Department (MET), Kuala Lumpur. Kuala Lumpur basically experiences a tropical rainforest climate, characterized by relatively stable temperatures year-round and a monsoon season typically occurring from the end of one year to the early part of the next. The meteorological data that was collected included weekly averages rainfall and global radiation , corresponding to the six-week exposure durations. The selected ageing period aimed to capture the early-stage degradation of MRE-EIP samples under natural environmental conditions, providing valuable context for assessing their physical and rheological performance over time (Fig. 2).

Morphological characterization

Surface and cross-sectional morphologies of MRE-EIP samples before and after natural weathering exposure were examined by using low vacuum scanning electron microscope (LVSEM), model JEOL IT300LV, located at Universiti Teknologi Malaysia, Kuala Lumpur, Malaysia. LVSEM was selected to accommodate the non-conductive SR matrix, allowing observation without the need for high-vacuum conditions while mitigating charging effects to the samples and observation process. Although the LVSEM mode reduces the need for conductive coatings, a thin platinum coating (~ 2 nm) was applied using a sputter coater (Auto Fine Coater JEC-3000FC) to enhance the image clarity and further minimize surface charging during high-resolution observation. Prior to the characterization, samples were prepared in a circular form (6 mm diameter) using a single-hole punch. Surface imaging was conducted on the as-cured top layer, while cross-sectional views were obtained by manually slicing the samples with a clean razor blade to expose the internal structure of the sample during observation. Samples were then mounted onto the standard SEM specimen stubs using conductive carbon tape to ensure proper grounding during vacuumed and imaging process. Imaging was performed at an accelerating voltage of 5 kV, with magnifications ranging from 200× to 1000×. A secondary electron detector (SED) was employed to capture the topographical features of the samples. The working distance was maintained between 10.4 mm and 11.1 mm, adjusted slightly across samples to accommodate variations in sample mounting height while preserving consistent imaging conditions.

Magnetic properties test

To evaluate the changes in magnetic properties due to environmental ageing, MRE-EIP samples were characterized using a vibrating sample magnetometer (VSM), Lake Shore Model 7404. Prior to each measurement, the VSM was calibrated using a nickel standard to ensure reliable and reproducible results. Measurements were conducted at room temperature on samples aged for 0, 3, and 6 weeks under natural weathering conditions, to capture both short-term and progressive magnetic changes. All samples were fabricated as disc-shaped specimens with 6 mm diameter and a mass of 0.072 g, ensuring consistent sample volume and geometry. During measurement, each sample was carefully aligned in the sensitivity coils to minimize positional errors. Magnetic field sweep from – 14 kOe to + 14 kOe was applied to ensure complete saturation and reversal of magnetic domains. This range was selected to adequately characterize the nonlinear magnetic behavior of soft ferromagnetic particles embedded in an elastomeric matrix. From the acquired hysteresis loops for each sample, M_s, coercivity (H_c), and remanent magnetization (M_r) values were extracted. These parameters were later critically analysed to detect changes

Fig. 2. Samples exposed to Kuala Lumpur's natural weathering.

associated with either iron particles, degradation at the particle-matrix interface, or particle agglomeration all of which could compromise the magneto-mechanical response of the MRE-EIP.

Rheological test

The viscoelastic and magneto-responsive properties of MRE-EIP were evaluated using an oscillation parallel plate rheometer (Physica MCR 302, Anton Paar, Graz, Austria) in oscillatory shear mode, with the aim of assessing the material's G' and MR effect following the natural weathering exposure. Disc-shaped samples (20 mm diameter) were prepared using a precision hollow punch and they were mounted between the rheometer's parallel plates under a constant normal force of 5 N to ensure consistent contact between plates and sample without over compression. All tests were performed at 25 °C, controlled by a Viscotherm VT2 unit that is equipped in the rheometer set up in order to eliminate thermal variability to the sample during testing. Rheological measurements were performed on three ($n = 3$) independently weathered samples for each exposure interval. For each sample, 3 repeated strain and magnetic field sweeps were conducted. The rheological protocol consisted of two stages: (1) a strain sweep test using a logarithmic shear strain that ramped from 0.001 to 10% at a constant frequency of 1 Hz. The test was conducted under discrete magnetic field conditions of 0, 0.18, 0.38, 0.57, 0.72 and 0.83 T generated by stepwise current inputs of 0, 1, 2, 3, 4, and 5 A, respectively in order to determine the change in G' and linear viscoelastic (LVE) region accordingly. Meanwhile in stage (2), a current sweep test was carried out at constant frequency of 1 Hz and shear strain that would be determined from stage (1), with the currents ramped linearly from 0 to 5 A, to evaluate the field-dependent modulation of G' of all MRE-EIP samples with magnetic fields. The magnetic field was applied perpendicular to the sample plane in order to induce maximum magnetic field to the sample upon shearing direction, a key mechanism underlying the greater MR effect of MRE-EIP.

Results and discussion

Magnetic properties of MRE-EIP samples

In magnetic properties, the magnetic moment, quantifies the strength of a particle's response to the applied field, indicating how strongly it is influenced by magnetic field[24]. Figure 3 presents the hysteresis loops for unaged and aged MRE-EIP samples, particularly W0, W3 and W6 while Table 1 summarises their corresponding magnetic properties including M_s, M_r and H_c. Over the six-week natural weathering exposure, the magnetic properties of MRE-EIP samples exhibited minor but measurable changes, reflecting the early-stage effects of environmental exposure to the EIP in the MRE-EIP samples. While the hysteresis loops of W0, W3 and W6 samples are visually similar, the subtle shifts in M_s, M_r, and H_c values may suggest a gradual response of the materials to environmental stressors.

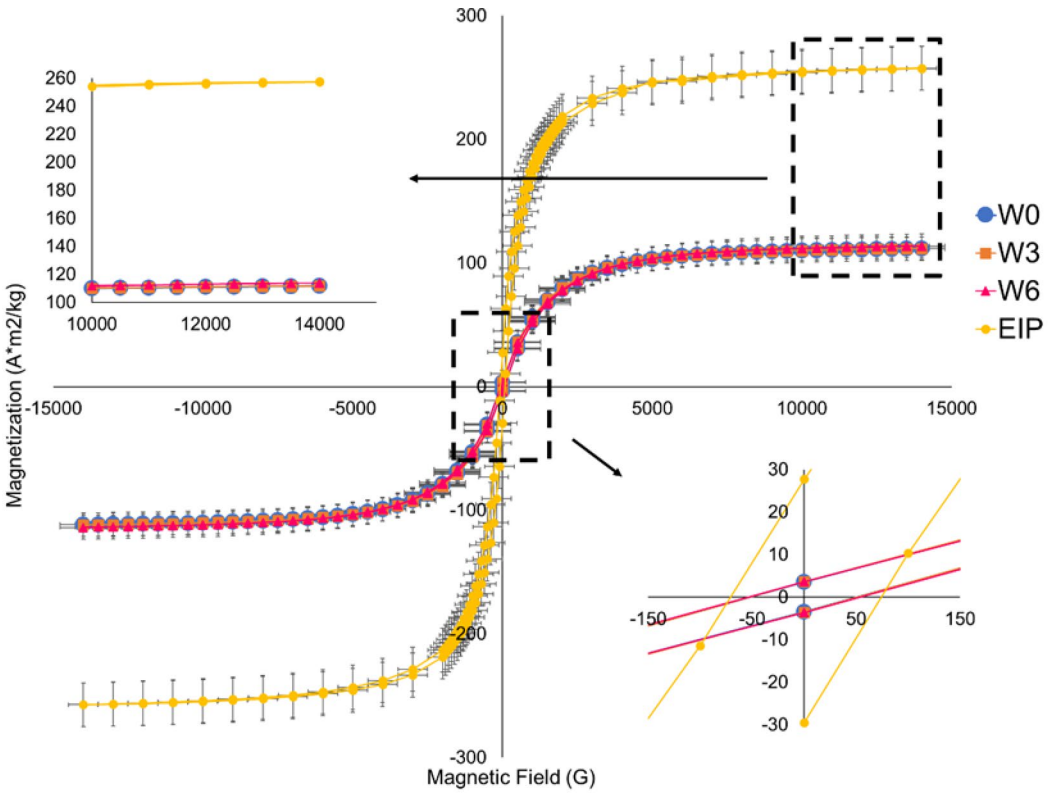

Fig. 3. Hysteresis loops of unaged (W0) and aged samples (W3 and W6) showing the magnetic properties of the samples.

Sample	Magnetization, M_s (Am^2/kg)	Remanence, M_r (Am^2/kg)	Coercivity, H_c (G)
Pure EIP	257.52	27.72	72.47
W0	111.63	3.53	51.78
W3	111.76	3.58	51.81
W6	113.79	3.62	53.69

Table 1. The summary of magnetic properties of unaged and aged MRE-EIP samples.

As shown in Table 1, the M_s of pure EIP was measured at 257.52 Am^2/kg, higher than the reported saturation magnetization of pure CIP particles ($M_s \approx 210.1$ Am^2/kg)[25]. The magnetic properties of the MRE-EIP samples shows M_s is 111.63 Am^2/kg, M_r is 3.53 Am^2/kg, and H_c is 51.78 G. These values are comparable to previously reported data for similar MRE-EIP systems, which exhibited M_s, M_r, and H_c at approximately at 123 Am^2/kg, 2.7 Am^2/kg, and 50 G respectively[15]. The slight differences in M_s and M_r can be attributed to variations in particle dispersion or fabrication conditions, whereas the H_c remains almost unchanged. Overall, the measured magnetic properties confirm that the embedded EIP contributes substantially to the magnetization of the composite, and that the material retains soft magnetic behavior suitable for field-responsive applications. On the other hand, weathered samples W3 and W6 display slightly higher values. This minimal increase is likely associated with the development of surface-level defects during weathering, which might partially expose the embedded EIP. The greater exposure of EIP allows more particles to actively contribute to the magnetic response, thereby elevating the overall magnetization effect. This interpretation is consistent with the morphological observations that will be discussed later. A comparable trend has also been reported in MRE-CIP under similar natural weathering, where surface degradation has facilitated the exposure of the particles[21]. In terms of M_r, the W0 sample records a value of 3.53 Am^2/kg, which is significantly higher than that typically reported for MRE-CIP[26]. This distinction is likely attributed to the irregular morphology and larger surface area of EIP. Shape anisotropy and internal strain effects, allows EIP to retain a greater fraction of magnetization when the external magnetic field is removed[27]. Upon exposure to natural weathering, the M_r values of W3 and W6 show a consistent increase, mirroring the trend observed for M_s. This correlation suggests that the progressive exposure of EIP on the sample's surface has not only enhanced their responsiveness to the applied field but also strengthens their remanent magnetization. In other words, as more EIP become accessible at the surface attributed to ageing effect, their capacity to remain magnetized after field removal increased, thereby leading to higher M_r values in the weathered samples. Similarly, the H_c values show a slight increment from W0 to W6, indicating a greater magnetic field intensity required to demagnetize the MRE-EIP samples. The phenomenon also can be correlated with the increased in M_r values with longer exposure durations. As the M_r values increased for sample W3 and W6, a greater magnetic field is required to demagnetize the remaining magnetization in the samples. The H_c value for the W0 sample is initially higher as compared to the MRE-CIP[26], attributed to the higher aspect ratio of the irregular EIP embedded in the elastomer[15]. Although the changes in magnetic properties may seem insignificant, the slight variations in magnetic properties have still highlighted the measurable influence of environmental weathering on the magnetic behaviour of MRE-EIP samples.

Strain sweep analysis of MRE-EIP samples

To investigate the effects of natural weathering on viscoelastic properties of MRE-EIP samples, the strain sweep tests were conducted on both unaged (W0) and aged samples (W1 to W6). As shown in Figs. 4a and b, the G' was recorded as a function of strain sweep under the off-state (0 T) and on-state conditions (0.83 T), respectively. Based on the plotted graphs, the LVE region for each MRE-EIP sample is determined, indicated by a constant G' over increasing strains. In this study, the LVE region is defined solely based on the response of the G', which is commonly adopted as the primary indicator for identifying LVE behaviour in MRE. It also defines the range where the deformation in the sample remains reversible linearly and does not significantly affect the network structure in the MRE-EIP samples. The LVE region is determined via Agirre-Olabide's method[28] in which the LVE limit is set at 10% deviation from the approximated straight horizontal line of the G'. This method was chosen as it aligns with the previous study that defines the elastic yield stress of MRE. The LVE strain limit is summarized in Table 2. Identifying the LVE region for MRE-EIP samples is crucial as it defines the strain range where the material responds elastically and linearly under deformation. Beyond this region, the material enters the non-linear viscoelastic region, where structural changes become non-linear and partially irreversible. At this region, the G' decreases with further increasing strains indicating that the material no longer responds linearly, and most notably as Payne effect. The Payne effect arises due to the breakage and reforming the physical interactions or bonds between the matrix and magnetic particles beyond the yield[28,29]. In addition, the Payne effect becomes more pronounced in the presence of a magnetic field, due to the intensified dipole-dipole interactions among the embedded particles as they align along with the field directions. Such alignment increases the resistance for internal structure to disrupt under the deformation[30].

Respective to Fig. 4, the LVE regions for MRE-EIP samples have progressively shortened with the increasing durations of natural weathering exposure. Marked with vertical red-dotted lines, the unaged sample (W0) exhibits the longest LVE range, both without (Fig. 4a) and with the magnetic field (Fig. 4b). However, as prolonged exposure to natural weathering, particularly over six weeks durations, a noticeable reduction in the LVE region is observed accompanied with the increased in the G'. This suggests a stiffening behaviour of the MRE-EIP, likely due to the environmental ageing effects such as UV radiation, raining, temperature fluctuations

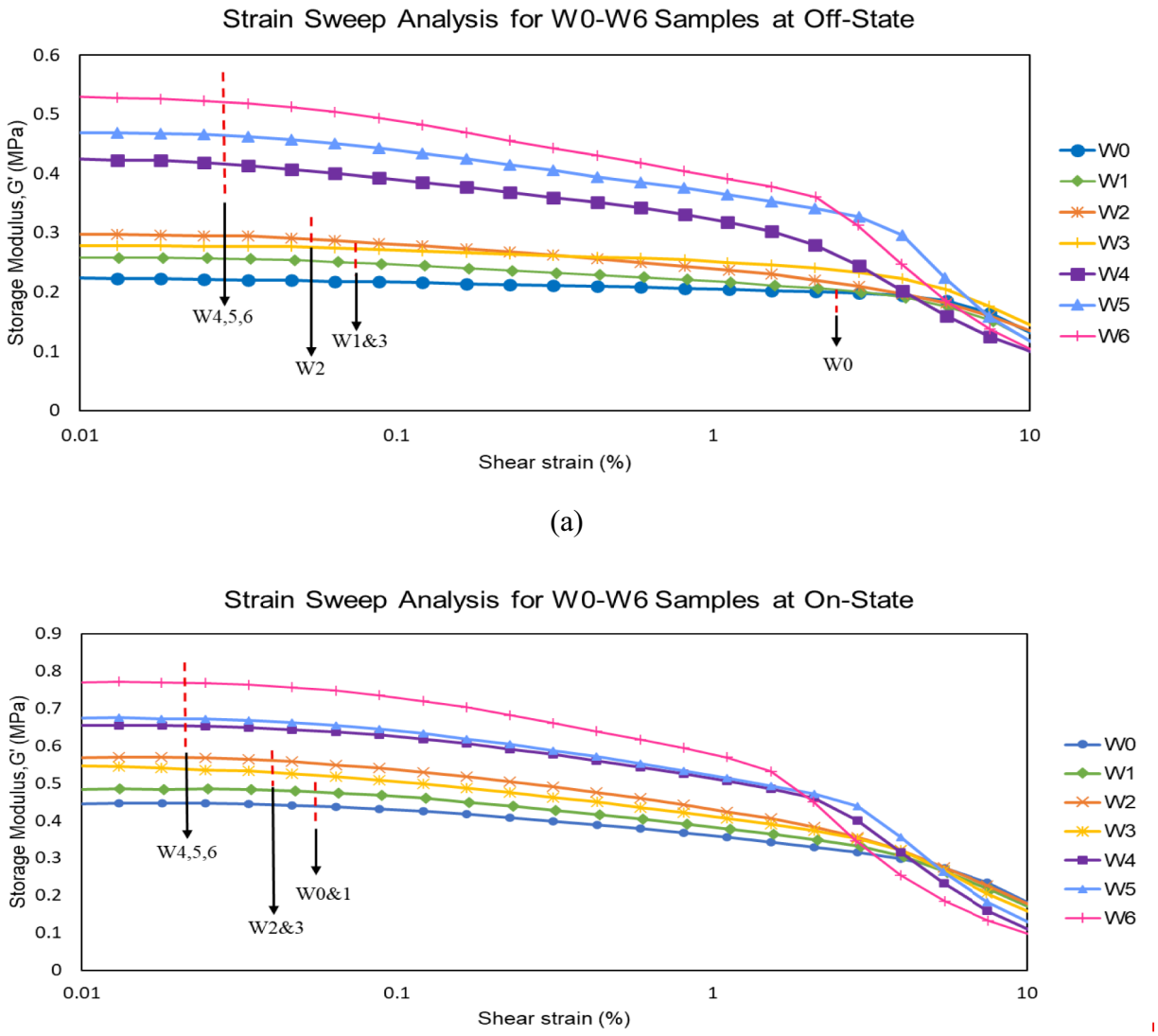

Fig. 4. Unaged (W0) and aged MRE-EIP samples for six weeks exposure (W1-W6) for (**a**) off-state (0 T) and (**b**) on-state (0.83 T) conditions.

Samples	LVE limit at off-state (%)	LVE limit at on-state (%)
W0	2.11	0.05
W1	0.06	0.05
W2	0.05	0.03
W3	0.06	0.03
W4	0.02	0.02
W5	0.02	0.02
W6	0.02	0.02

LVE limit of MRE-EIP samples.

and maybe oxidation that have altered the molecular bonding of the SR matrix, promoting crosslinking within the phase and reducing molecular mobility in the polymer chains, leading to shorter LVE region[31]. The reduction in the LVE region also synonym with the increment of G'. As the MRE-EIP becomes stiffer with higher G', the internal structure reaches the non-linear behaviour more quickly under given strains. Thus, it can no longer

tolerate the larger deformations without structural changes and loses its ability to respond elastically at lower strain levels. The LVE region then ends earlier, as shown in Fig. 4a. However, a slight recovery of the LVE region was observed for sample W3. This behaviour is interpreted as a transient softening response associated with short-term environmental exposure, which is elevated rainfall during the third week. This behaviour reflects the simultaneous influence of two ageing mechanisms acting over different timescales. Short-term environmental exposure, particularly elevated rainfall, can induce reversible softening of the matrix through moisture absorption and plasticisation . In contrast, prolonged exposure to UV radiation promotes irreversible stiffening via additional crosslinking and surface hardening of the polymer network. The observed response at W3 therefore represents a temporary dominance of the short-term softening mechanism, which is gradually overtaken by the progressive stiffening effect with extended weathering duration. Such a phenomena can soften the matrix and slightly extend its ability to sustain larger strains in linear deformation. Additionally, the application of 0.83 T (on-state condition) has further reduced the LVE limit across all the samples as shown in Fig. 4b. This effect is more pronounced in weathered samples, likely implying a dual stiffening response resulting from both weathering-induced embrittlement and the interactions between EIP with magnetic field. These cause the particle-matrix bonding to become more rigid, leading to a loss of linear response and a reduced capacity of the MRE-EIP to sustain greater strains[21]. The shorter LVE limits in different MRE-EIP samples are marked with red-dotted lines in Fig. 4b.

Table 2

In W0, particularly at 0 T (Fig. 4a), the sample exhibited an initial G' of 0.22 MPa. This value lies within the same order of magnitude as that reported for MRE-CIP system, containing 70 wt.% of the particles which is about 0.21 MPa[21]. This is notable to mention that the unique morphology of EIP, which possess higher surface area and irregular geometry has promoted better cross-linking between the particles and SR matrix, which could partially enhance the G' with lower filler concentration[14,15]. Over the weathering exposure meanwhile, the G' exhibited distinct changes over different exposure periods. The interpretation of initial G' over six weeks exposures that were extracted from Fig. 4, along with the average global radiation (UV) and rainfall data from MET department, is presented in Figs. 5 and 6, respectively. For the first two weeks exposure, the increase in the initial G' was observed for W1 and W2, approximately 0.26 MPa and 0.30 MPa, respectively. The increase in the G' shall be corresponded to the UV radiation that was induced to the samples within the periods as presented in Fig. 5, as the UV radiation promotes cross-linking in the SR matrix, resulting in a stiffer characteristic of the overall MRE-EIP. These observations are consistent with findings reported by Johari et al.[21], who documented about the increment in stiffness of MRE-CIP after natural weathering, attributing the changes in the formation of additional cross-links in the polymer chains of SR .

A non-monotonic trend was observed during the third week (W3), where G' exhibited a slight decline. This temporary reduction in G' may be associated with elevated rainfall, which can introduce short-term softening effects in SR matrix as illustrated in Fig. 4, leading to moisture absorption by the SR matrix. The more absorbed water in that week might cause swelling of the matrix, temporarily disrupt the intermolecular interactions, and reduce the stiffness of MRE-EIP. This softening mechanism also might be similar with the observation done by Zaini et al.[23], who reported that immersion of MRE-CIP in a seawater led to a measurable reduction in the G'. This degradation is likely due to the water-induced plasticisation and hydrolysis, which increased the mobility of polymer chains and weakened the internal bonding of SR matrix. Despite this decline, the G' remains above than that of the unaged sample (W0), suggesting that UV-induced cross-linking in the third week continued to exert a reinforcing effect on W3, highlighting the competing environmental factors onto the sample. Meanwhile, for the continuous of four to six weeks exposure, the G' of W4, W5 and W6 further increased, likely due to sustained UV exposure combined with lower average rainfall in weeks 4 and 5, which may have promoted

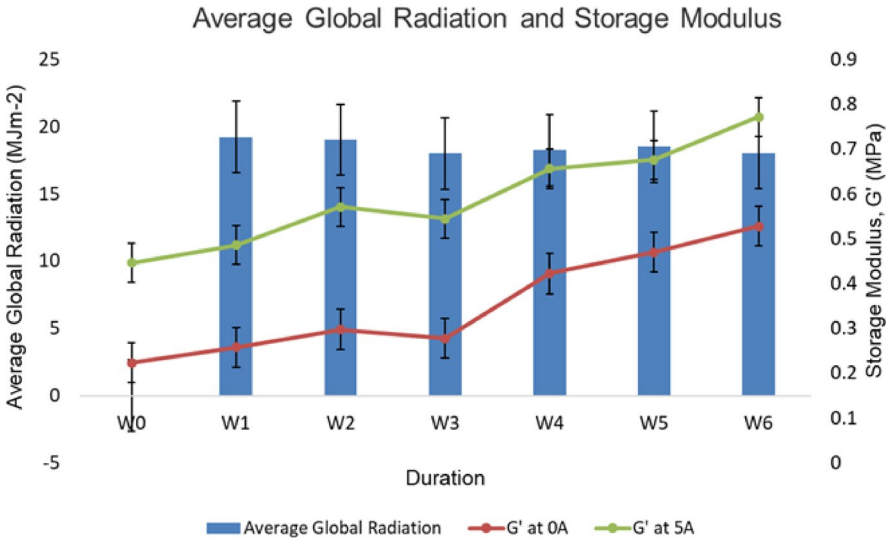

Fig. 5. Average global UV radiation and changes in the initial G' of MRE-EIP at off- and on-state conditions.

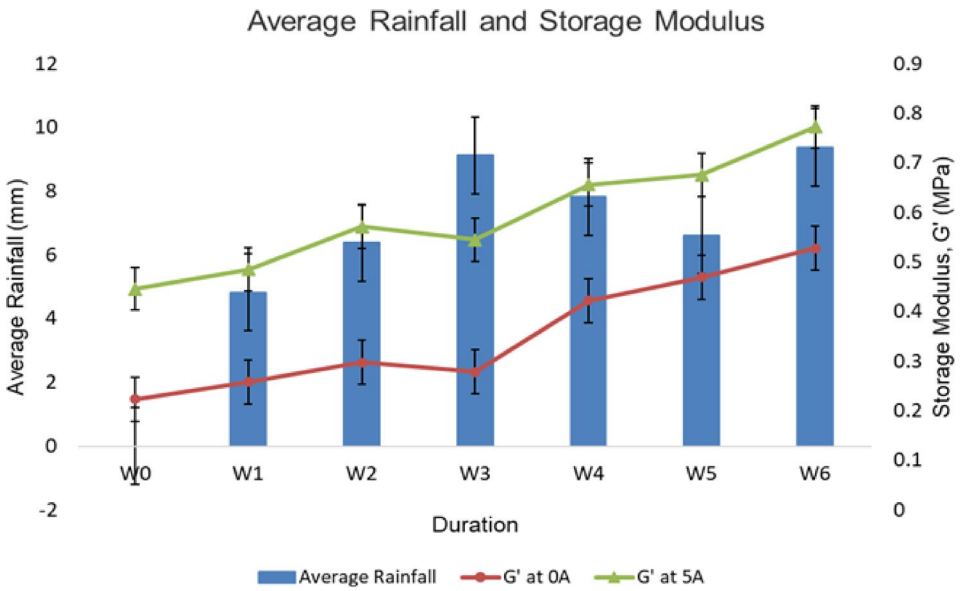

Fig. 6. Average rainfall and changes in the initial *G'* of MRE-EIP at off- and on-state conditions.

progressive cross-linking in the SR matrix. Notably, although W6 experienced the highest average rainfall among all exposure periods, an increase in G' was still observed. This indicates that the ageing response is governed by competing mechanisms rather than moisture-induced plasticisation alone. With prolonged and continuous natural weathering, hardening mechanisms become dominant. These are likely associated with additional crosslinking within the SR induced by continuous environmental exposure. As these processes progressively outweigh the softening effect of absorbed moisture, the net response at W6 is an increase in G'. As discussed previously, this stiffening behaviour in the samples are accompanied by a further narrowing of the LVE region, indicating a transition towards increased brittleness and reduced elasticity. This behaviour reflects a more rigid and less flexible polymer network in the MRE-EIP samples resulting from prolonged ageing effects. It should be noted that the present analysis focuses on stiffness-dominated viscoelastic behaviour derived from G' trends, and therefore the discussion of softening or stiffening effects is limited to relative changes rather than comprehensive viscoelastic dissipation mechanisms.

In contrast to the changes in the initial G' at the off-state condition, the induced magnetic field of 5 A or 0.83 T to the aged samples showed substantial changes in the viscoelastic response of the MRE-EIP. Under the on-state condition, the G' values approximately doubled compared to those in the off-state condition. Exhibiting a similar pattern, the increase is attributed to the alignment of magnetic dipole moments in the EIP with the direction of magnetic field, which strengthens the magnetic forces between the particles and enhances the particle–matrix interactions[32]. Besides, the high aspect ratio and irregular shape of EIP has further improved the mechanical stiffness and resistance of MRE-EIP to deformation. This indicates that the alteration or degradation in MRE-EIP properties due to ageing effect can be mitigated by the application of magnetic fields. The findings highlight the dual nature of environmental weathering, which are UV exposure that acts as a stiffening agent through additional crosslinking, while moisture from rainfall promotes softening via plasticisation . The application of a magnetic field meanwhile consistently reinforces the network structure, suggesting its potential to compensate for degradation during prolonged environmental exposure.

Magnetic field sweep analysis of MRE-EIP samples

During a shear test of MRE-EIP samples under the influence of magnetic fields, the EIP within the MRE-EIP would be magnetised due to dipole-dipole interactions within and among the particles. In response to the magnetic field, dipole-dipole interactions cause the particles to align along the field direction. This alignment restricts the deformation of the SR matrix and contributes to increased stiffness. As a result, additional effort is required for these magnetic particles to oscillate from their minimal energy state, leading to a field-dependent shear modulus that varies with the changes in magnetic field strength. This field-dependent behavior allows the shear modulus to be tuned in real time, which is advantageous for applications requiring adaptive stiffness control. In this study, the magnetic field sweep is used to evaluate the stiffness dominated magnetorheological (MR) effect of MRE-EIP through changes in G'. The key parameter for assessing the change in G' is referred to as MR effect[33].

Figure 7 illustrates the variation in G' of MRE-EIP samples as a function of magnetic field strength after six weeks of weathering. Here, G'_0 represents the initial modulus at 0 T, while G'_{max} denotes the maximum modulus under the maximum magnetic flux density applied (0.83 T). An increase in G' with rising magnetic flux density is observed, attributed to the stronger magnetic forces between the EIP as magnetic field strength increases. These magnetized EIP strengthen particle-particle and particle-matrix interactions, which increase the elastic resistance of the MRE-EIP to deformation under applied magnetic fields[34]. This behaviour is consistent with the

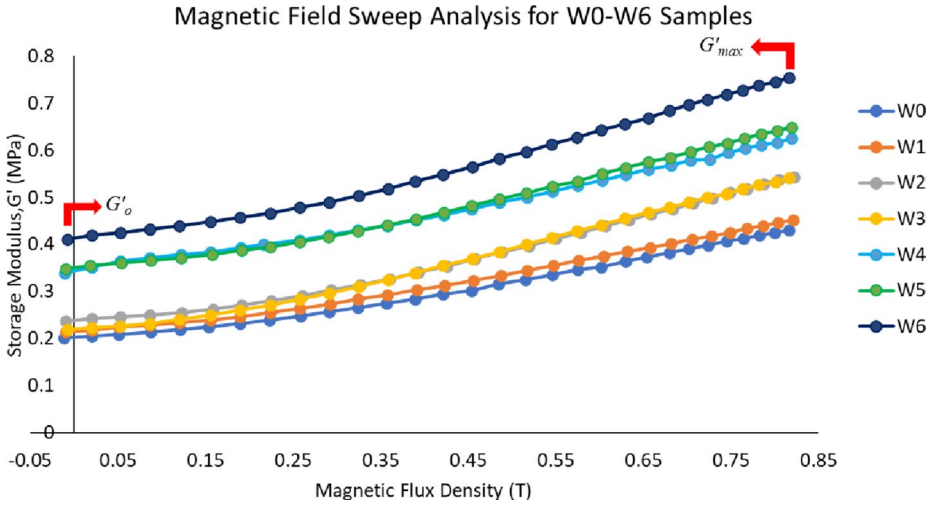

Fig. 7. Magnetic fields sweep analysis for sample W0 to W6 that exposed to different weekly durations.

Weekly sample	ΔG' (MPa)
W0	0.23 ± 0.006
W1	0.24 ± 0.006
W2	0.31 ± 0.006
W3	0.32 ± 0.02
W4	0.29 ± 0.03
W5	0.30 ± 0.01
W6	0.34 ± 0.01

Table 3: ΔG' of MRE-EIP samples underwent weekly exposure durations.

VSM magnetization trend, indicating that the field-induced stiffening of MRE-EIP is predominantly controlled by magnetized particle interactions rather than solely by the applied magnetic field magnitude. All MRE-EIP samples exhibited similar behaviour. Table 3 tabulates the absolute MR effect, $\Delta G'$ of MRE-EIP samples after exposed to natural weathering in different durations. The $\Delta G'$ reflects how natural weathering influences the range of magnetically induced stiffness variation of MRE-EIP samples under tunable magnetic fields.

In brief, the $\Delta G'$ of the seven samples exhibits a non-monotonic trend over the six-week ageing periods. From W0 to W3, a progressive increase in $\Delta G'$ is observed. During this period, natural weather ageing effect leads to an increase in the G'_0 of the MRE-EIP, reflecting the gradual stiffening of the elastomer matrix. Despite this baseline stiffening, the field-induced G' continues to increase with magnetic flux density up to 0.83 T. This indicates that the applied magnetic field remains effective in promoting particle-particle interactions and reinforcing the stiffness of MRE-EIP. Consequently, the observed increase in $\Delta G'$ is primarily attributed to the changes in matrix-particle interactions rather than a loss of magnetic responsiveness. The samples that have been exposed to natural weathering experienced elevated UV radiation and heat which likely initiates and promotes cross-linking within the SR matrix. These additional cross-links improved the structural stability of the matrix, making it stiffer and less deformable which improves the mechanical constraint on the EIP. As a result, when a magnetic field is applied, the magnetized particles are more effectively coupled to the rigid matrix, allowing magnetic interaction forces to be transmitted more efficiently and leading to a larger increase in G' under the applied field. In fact, the maximum $\Delta G'$ is recorded in W3, coinciding with a significant increase in the environmental rainfall as presented in Fig. 6. The moisture content during this period may be associated with a transient reduction in matrix stiffness, which coincides with a marginal decrease in the initial G' of the W3 sample compared to W2. The condition also allowed slight adjustment in the particle's alignment and interparticle magnetic interactions upon the field application. Besides, the irregular shape and high packing density of the EIP further contribute to the enhanced dipole interaction strength and the formation of field-induced particles networks[16], thus, enhancing the G' response. In contrast, the W4 sample showed a notable decline in $\Delta G'$. This reduction may be attributed to progressive ageing-induced stiffening of the matrix, which restricts particle mobility and limits the formation and reconfiguration of field-induced EIP structures under magnetic excitation, thereby reducing the incremental modulus enhancement. It appears that prolonged UV exposure and moisture may have disrupted the formation of field-induced particle structures and particle-matrix interfacial bonding, thereby weakening the MR effect. Then, a moderate recovery in $\Delta G'$ is observed in W5 to W6 samples. This varying trend highlights the importance of understanding competing environmental influences on MR properties, which is critical for designing durable MRE-EIP systems for long-term outdoor applications. The role of magnetic field applications

is also crucial in adjusting the responsiveness and performance of the material. Although an increase in the $\Delta G'$ is observed with increasing weathering duration, this trend is primarily attributed to the increase in the G'_0 resulting from ageing-induced stiffening of the MRE-EIP matrix. Despite the higher absolute change in G' under an applied magnetic field, the material's ability to further change its stiffness is progressively reduced with prolonged environmental exposure. This indicates that environmental ageing enhances the baseline rigidity of the MRE-EIP while simultaneously diminishing its responsiveness to magnetic-field-induced particle interactions.

Morphology characterization of MRE-EIP samples

Figure 8 presents the surface morphology of MRE-EIP samples before and after exposed to natural weathering, in different exposed durations. This study presents the first documented observation of morphological changes in MRE-EIP under these conditions, using LVSEM. Observation and analysis of W0 sample reveals a smooth,

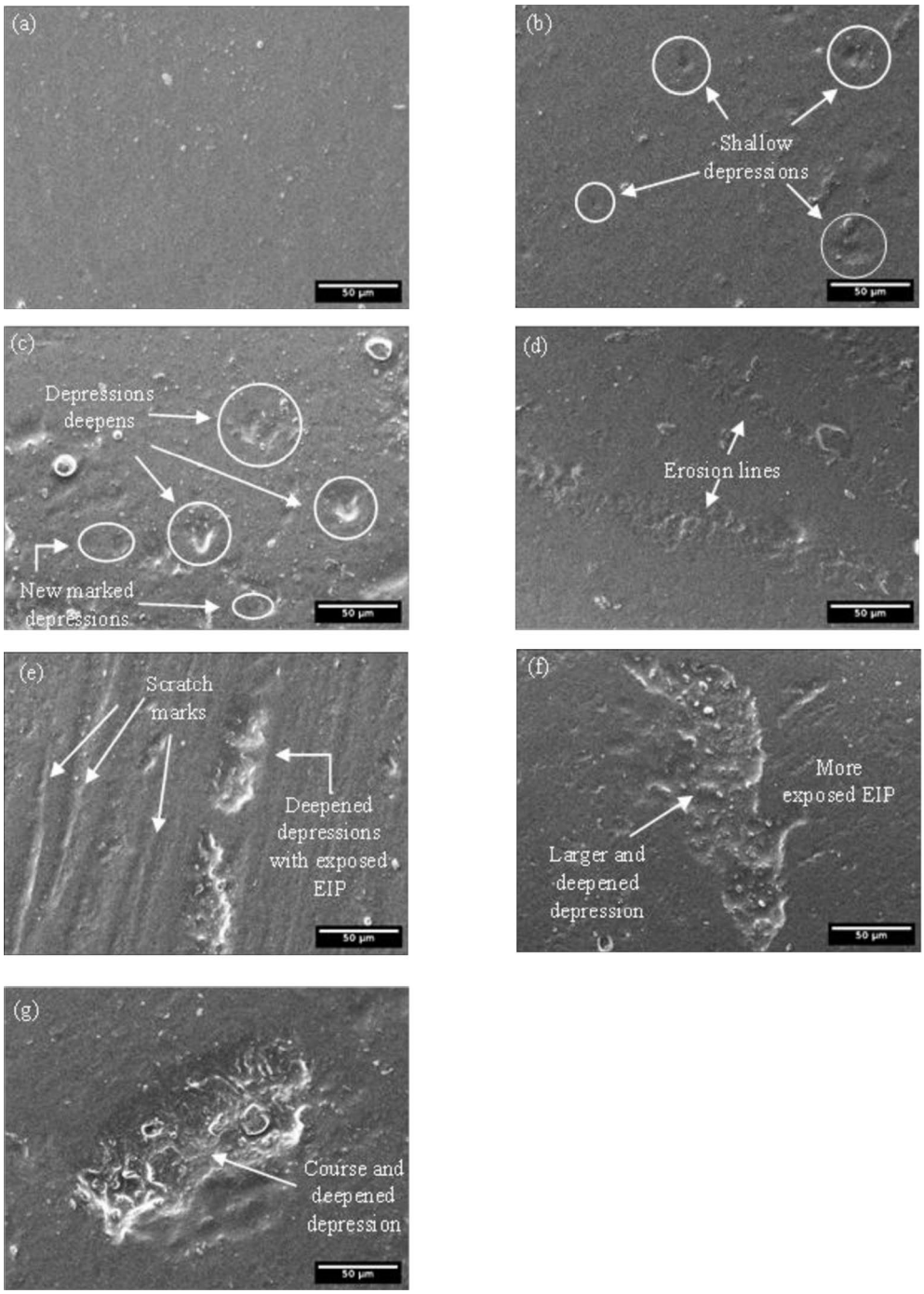

Fig. 8. Surface morphology of MRE-EIP samples for (**a**)W0, (**b**) W1, (**c**) W2, (**d**) W3, (**e**) W4, (**f**) W5 and (**g**) W6.

defect-free surface with minor EIP fragments present, as shown in Fig. 8a. However, after one week of ageing effect, the initial surface defects begin to appear. Fig. 8b highlights the emergence of small, round, and shallow depression on W1 sample, marking the onset of surface deterioration. Then, by two weeks exposure, particularly W2 in Fig. 8c, these depressions deepen with more EIP being visible on the surface of MRE-EIP. New depressions have also been developed simultaneously, making more marked defects have been observed. Following three weeks of exposure periods, erosion lines begin to form, as depicted in Fig. 8d for sample W3. A closer analysis of these lines shows an increasing number of depressions, deepened which eventually extended across the surface. The formation of these lines is likely caused by the runoff of rainwater across the SR's surface, which gradually removes degraded material along its flow paths, leading to visible erosion patterns. Then, by the fourth week of weathering exposure, Fig. 8e shows the development of multiple scratch-like marks, accompanied with the continued deepening of the existing depressions. These marks are likely caused by the abrasive impact of wind-driven dust and particulate matters, which could rub and cut into the outer matrix layer. In MRE-EIP, such abrasion has not only removed the outer surface layer but also caused exposure of the embedded particles, as shown in the figure. The observed depressions then have been intensified after five weeks of ageing effect, as illustrated in sample W5 in Fig. 8f, indicating continuous penetration of rainwater and degradative effects by UV radiation. Based on Fig. 8f, small particles which represent the EIP are observed on the defected area. This persisted at six weeks of exposure as shown in Fig. 8g, with the course depressions becoming deeper and the particles have been increasingly exposed (W6). The increased particle exposure corresponds to the improvement in the magnetic properties of the exposed samples, as discussed in Sect. 3.1. Overall, as the exposure durations increased, the depression that initiated and developed on the surface of MRE-EIP sample were growing larger and deeper.

As has been mentioned, the defects began as shallow depression which progressively grew deeper as the duration of weathering exposure increased. This phenomenon can be attributed to the combined effects of rainwater penetration, UV radiation from sunlight, and wind-blown. UV radiation primarily attacks the surface of MRE-EIP, breaking down polymer chains and causing the surface roughening. Rainwater, which often contains dissolved gases can have a pH as low as 5.5[22]. The slightly acidic nature of rainwater then accelerates hydrolytic and oxidative degradation chemically, further weakening the surface and promoting the formation of depressions. These phenomena are illustrated in Fig. 9, for W0 to W1. Over the course of continuous exposure, the alternating UV radiation and rainwater penetration into these microcracks or amorphous domains in the samples have further intensified the effects, leaving behind larger and deeper depressions. The rainwater runoff also removed loosened polymer fragments physically, which explains the presence of erosion lines observed in samples W2 to W6. Wind added another mechanical factor by carrying dust and particulate matter that abrasively eroded the surface and dislodged already-degraded material. This factor may cause the formation of scratch marks found in W4 onwards, which also led to the exposure of the EIP. These combined chemical and mechanical processes resulted in the progressive deepening of the depressions, formation of erosion lines and scratch marks and those are often localized likely due to higher susceptibility of the amorphous phase of SR (matrix) compared to its crystalline domains. This site-specific degradation indicates that MRE-EIP exhibited the anisotropic behaviour, with localized surface defects developing preferentially in more vulnerable regions[35].

In addition to the morphological characterizations, the cross-sectional area of W0 and W6 are analysed as presented in Fig. 10a and b, respectively. After six weeks of weathering exposure, the tomography of W6 sample (Fig. 10b) revealed no discernible differences as compared to the unexposed sample (Fig. 10a), indicating that the internal microstructure of MRE-EIP has remained intact. This finding suggests that throughout the degradation process, if defects have been initiated at the surface, those have not yet propagated into the interior regions of the MRE-EIP within the six-week timeframe. In other words, the bulk matrix of the elastomer and embedded particles have retained their original arrangement and bonding. This structural stability is also consistent with the VSM results as in Fig. 3 and Table 1, which showed negligible variations in the magnetic properties after six weeks weathering exposure. Interestingly, despite this microstructure stability, a slight increase in the $\Delta G'$ was observed from the rheological measurements, suggesting that the rheometer may be more sensitive to the surface modifications induced by the early-stage weathering. These surface-level alterations could locally influence the particle-matrix interactions, leading to minor changes in magnetic field response. To confirm whether such effects extend to the overall functional performance of MRE-EIP, future studies involving real-device testing are recommended to assess the MR effect across the entire material volume.

Conclusion

This study presents a systematic evaluation of the early-stage environmental degradation of MRE-EIP after six weeks of natural weathering. Combined magnetic, rheological, and morphological analyses revealed that short-term exposure have primarily affected the surface morphology and viscoelastic responses, while bulk microstructure and magnetic properties remained largely intact. Magnetic measurements showed slight increment in M_s (111.63–113.79 Am^2/kg), M_r (3.53 to 3.62 Am^2/kg) and H_c (51.78 to 53.69 G), which correlate to the exposed particles on the surface of samples upon ageing effect. Rheological findings meanwhile demonstrating stronger weathering effects. The G' at 0 T rose from 0.22 MPa (W0) to 0.53 MPa (W6) as the materials become stiffer which may be attributed to combined effects of UV radiation which typically induced cross-linking in the elastomer and rainfall that provides plasticisation effects. A transient softening was observed in W3 likely due to greater rainfall in that week. Under 0.83 T, G' nearly doubled to 0.77 MPa in W6, confirming the magnetic reinforcement although the LVE region of W6 has been shortened with ageing, signalling reduced elasticity and early embrittlement of the sample. Magnetic field sweeps showed a non-monotonic $\Delta G'$, increasing to 0.32 MPa in W3 before declining, followed by a partial recovery at later ageing stages. Morphological observations then confirmed the progressive surface defects, while cross-sections showed internal structure remain intact, consistent with stable magnetic properties measurement. Overall, the natural weathering induced measurable

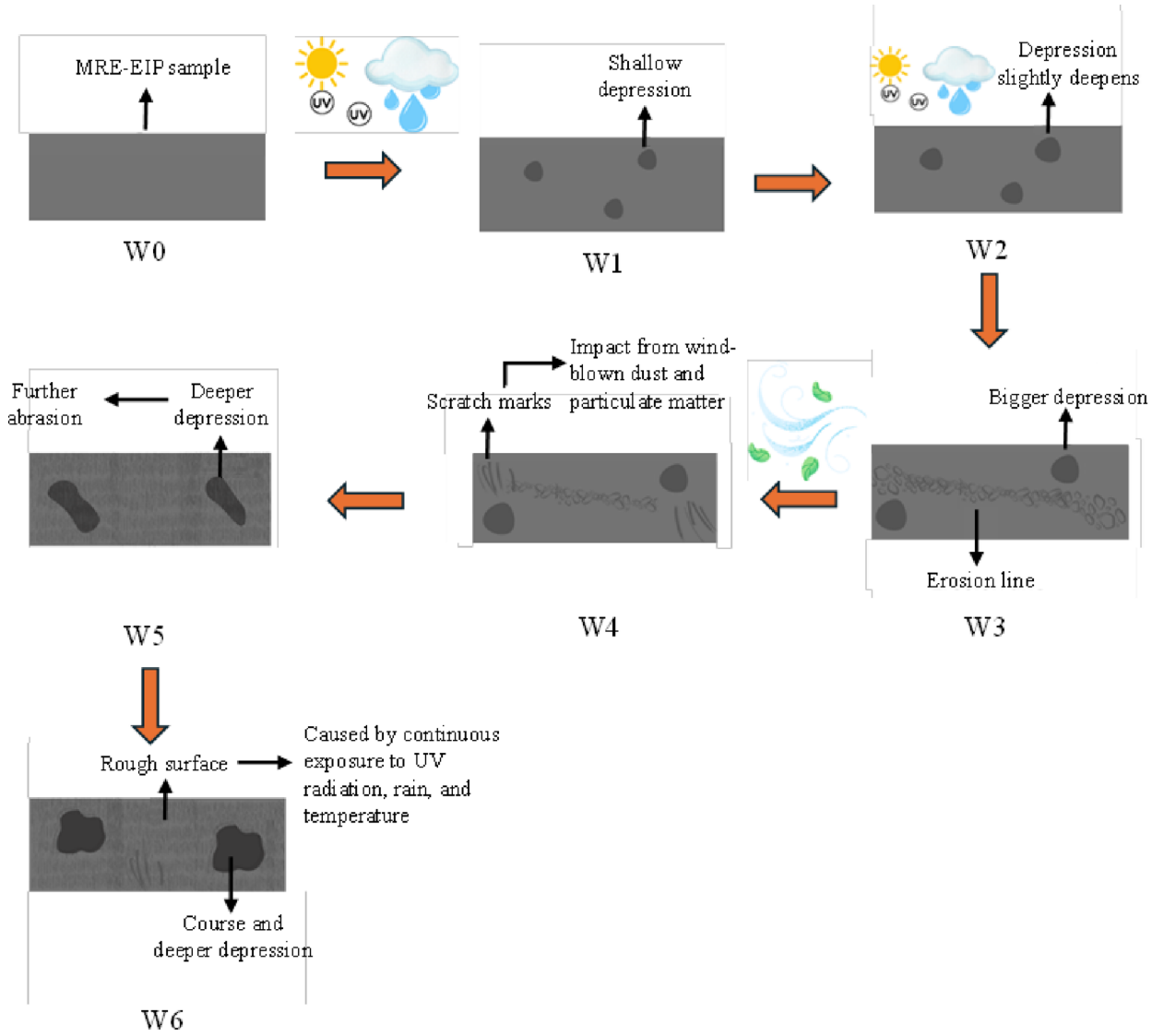

Fig. 9. Schematic representations of natural weathering effects on the MRE-EIP samples across different durations.

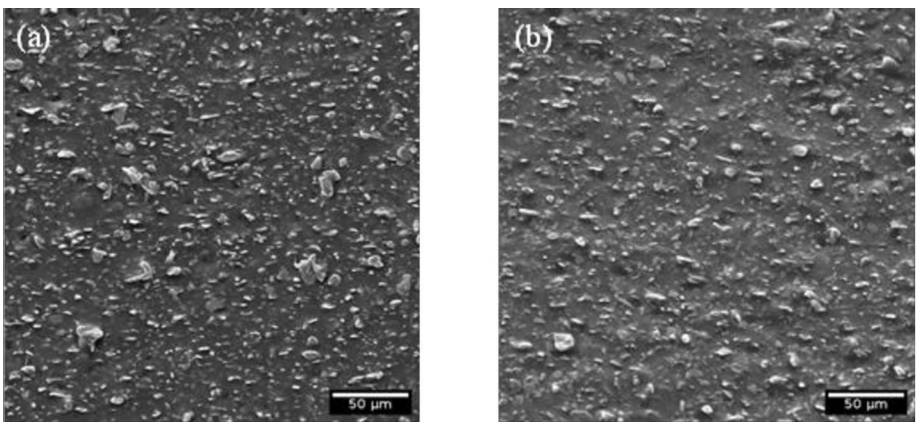

Fig. 10. Cross-sectional area of MRE-EIP samples for (**a**) W0 and (**b**) W6.

surface deterioration and stiffness increased but preserved bulk magnetic function, underscoring short-term stability yet highlighting early signs of long-term vulnerability. Future work will focus on controlled ageing experiments that isolate the effects of individual environmental factors, such as UV radiation, moisture, and thermal cycling. This will enable decoupling of the complex synergistic effects observed under combined natural weathering and provide a deeper understanding of the mechanisms governing early-stage degradation of MRE-EIP systems.

Data availability

The data presented in this study are available on request from the corresponding author.

Received: 6 November 2025; Accepted: 14 January 2026
Published online: 30 January 2026

References

1. Hafeez, M. A., Usman, M., Umer, M. A. & Hanif, A. Recent progress in isotropic magnetorheological elastomers and their properties: A review. *Polym. (Basel)*. **12** (12), 3023. https://doi.org/10.3390/polym12123023 (2020).
2. Chen, Z. et al. Investigation of a new metamaterial magnetorheological elastomer isolator with tunable vibration bandgaps. *Mech. Syst. Signal. Process.* **170**, 108806. https://doi.org/10.1016/j.ymssp.2022.108806 (2022).
3. Brancati, R., Di Massa, G., Pagano, S. & Santini, S. A magneto-rheological elastomer vibration isolator for lightweight structures. *Meccanica* **54**, 1–2. https://doi.org/10.1007/s11012-019-00951-2 (2019).
4. Kim, G. W., Kim, S. & Choi, H. J. Enhanced performance of nano-sized maghemite added carbonyl iron-based magnetorheological soft elastomer. *J. Magn. Magn. Mater.* **560**, 169659. https://doi.org/10.1016/j.jmmm.2022.169659 (2022).
5. Zhang, G. et al. Effects of graphene oxide on microstructure and mechanical properties of isotropic polydimethylsiloxane-based magnetorheological elastomers. *Rheol Acta*. **61** (3), 215–228. https://doi.org/10.1007/s00397-022-01329-0 (2022).
6. Vatandoost, H., Rakheja, S. & Sedaghati, R. Effects of iron particles' volume fraction on compression mode properties of magnetorheological elastomers. *J. Magn. Magn. Mater.* **522** (167552). https://doi.org/10.1016/j.jmmm.2020.167552 (2021).
7. Garcia-Gonzalez, D., Moreno, M. A., Valencia, L., Arias, A. & Velasco, D. Influence of elastomeric matrix and particle volume fraction on the mechanical response of magneto-active polymers. *Compos. B Eng.* **215**, 108796. https://doi.org/10.1016/j.compositesb.2021.108796 (2021).
8. Tian, T. & Nakano, M. Fabrication and characterisation of anisotropic magnetorheological elastomer with 45° iron particle alignment at various silicone oil concentrations. *J. Intell. Mater. Syst. Struct.* **29** (2), 151–159. https://doi.org/10.1177/1045389X17704071 (2018).
9. Yao, J., Yang, W., Scarpa, F. & Li, Y. Magnetorheological elastomers with particle chain orientation: modelling and experiments. *Smart Mater. Struct.* **10** (9), 22408–22418. https://doi.org/10.1088/1361-665X/ab2e21 (2019).
10. Nam, T. H., Petríková, I. & Marvalová, B. Experimental characterization and viscoelastic modeling of isotropic and anisotropic magnetorheological elastomers. *Polym. Test.* **81**, 106272. https://doi.org/10.1016/j.polymertesting.2019.106272 (2020).
11. Tagliabue, A., Eblagon, F. & Clemens, F. Analysis of styrene-butadiene based thermoplastic magnetorheological elastomers with surface-treated iron particles. *Polym. (Basel)*. **13** (10). https://doi.org/10.3390/polym13101597 (2021).
12. Liu, T. & Xu, Y. Magnetorheological Elastomers: Materials and Applications, In *Magnetorheological Elastomers: Materials and Applications*, IntechOpen https://doi.org/10.5772/intechopen.85083, (2019).
13. Kumar, V. & Lee, D. J. Iron particle and anisotropic effects on mechanical properties of magneto-sensitive elastomers. *J. Magn. Magn. Mater.* **441**, 105–112. https://doi.org/10.1016/j.jmmm.2017.05.049 (2017).
14. Alam, M. N., Kumar, V., Lee, D. J. & Choi, J. Magnetically active response of acrylonitrile-butadiene-rubber-based magnetorheological elastomers with different types of iron fillers and their hybrid. *Compos. Commun.* **24**, 100657. https://doi.org/10.1016/j.coco.2021.100657 (2021).
15. Patel, D., Upadhyay, R. V. & Mazlan, S. A. Particle-reinforced elastomer model to analyse viscoelastic properties of flake-shaped electrolyte iron particle-based magnetorheological elastomer. *Smart Mater. Struct.* **32** (9). https://doi.org/10.1088/1361-665X/ace573 (2023).
16. Kumar, V. & Lee, D. Mechanical properties and magnetic effect of new magneto-rheological elastomers filled with multi-wall carbon nanotubes and iron particles. *J. Magn. Magn. Mater.* **482**, 329–335. https://doi.org/10.1016/j.jmmm.2019.03.075 (2019).
17. Siddiqui, M. N. et al. Durability study of asphaltene-reinforced HDPE and LDPE composites under UV irradiation and local weathering exposure, *Polymer Bulletin*, vol. 78, no. 8, pp. 4487–4503, (2021). https://doi.org/10.1007/s00289-020-03326-w
18. Ismail, H. & Awang, M. Natural weathering of polypropylene and waste tire dust (PP/WTD) blends. *J. Polym. Environ.* **16** (2), 147–153. https://doi.org/10.1007/s10924-008-0087-6 (2008).
19. de Oliveira, G. L., Ariza Gomez, A. J., Caire, M., Vaz, M. A. & Costa, M. F. Characterization of seawater and weather aged polyurethane elastomer for bend stiffeners, *Polym. Test*, vol. 59, pp. 290–295, (2017). https://doi.org/10.1016/j.polymertesting.2017.02.012
20. Noriman, N. Z., Ismail, H. & Rashid, A. A. Natural weathering test of styrene butadiene rubber and recycled acrylonitrile butadiene rubber (SBR/NBRR) blends. *Polym. Plast. Technol. Eng.* **49** (7), 731–741. https://doi.org/10.1080/03602551003664552 (2010).
21. Johari, M. A. F. et al. Natural weathering effects on the Mechanical, Rheological, and morphological properties of magnetorheological elastomer (MRE) in tropical climate. *Int. J. Mol. Sci.* **23** (17), 9929. https://doi.org/10.3390/ijms23179929 (2022).
22. Johari, M. A. F. et al. Morphological features of magnetorheological elastomer degradation under a natural weathering environment. *Sci. Rep.* **14** (1), 1–14. https://doi.org/10.1038/s41598-024-51736-x (2024).
23. Zaini, N. et al. Deterioration behavior of aged magnetorheological elastomer under harsh marine environment. *Express Polym. Lett.* **18** (7), 728–741. https://doi.org/10.3144/expresspolymlett.2024.54 (2024).
24. Khairi, M. H. A. et al. Enhancement of Magneto-Induced modulus by the combination of filler and plasticizer Additives-Based magnetorheological elastomer. *Materials* **15** (18), 1–12. https://doi.org/10.3390/ma15186396 (2022).
25. Li, C. et al. Mechanism-Oriented analysis of Core–Shell structured CIP@SiO2 magnetic abrasives for Precision-Enhanced magnetorheological Polishing. *Micromachines (Basel)*. **16** (5). https://doi.org/10.3390/mi16050495 (2025).
26. Aziz, S. A. A. et al. Loss factor behavior of thermally aged magnetorheological elastomers. *Materials* **14** (17). https://doi.org/10.3390/ma14174874 (2021).
27. Mohamad, N. et al. A comparative work on the magnetic field-dependent properties of plate-like and spherical iron particle-based magnetorheological grease. *PLoS One*. **13** (4), 1–16. https://doi.org/10.1371/journal.pone.0191795 (2018).
28. Agirre-Olabide, I., Berasategui, J., Elejabarrieta, M. J. & Bou-Ali, M. M. Characterization of the linear viscoelastic region of magnetorheological elastomers. *J. Intell. Mater. Syst. Struct.* **25** (16), 2074–2081. https://doi.org/10.1177/1045389X13517310 (2014).
29. Salem, A. M. H., Ali, A., Bin Ramli, R., Muthalif, A. G. A. & Julai, S. Effect of carbonyl iron particle types on the structure and performance of magnetorheological elastomers: A frequency and strain dependent study. *Polym. (Basel)*. **14** (19), 4193. https://doi.org/10.3390/polym14194193 (2022).

30. Burgaz, E. & Goksuzoglu, M. Effects of magnetic particles and carbon black on structure and properties of magnetorheological elastomers. *Polym. Test.* **81**, 106233. https://doi.org/10.1016/j.polymertesting.2019.106233 (2020).
31. Tong, Y., Dong, X. & Qi, M. Payne effect and damping properties of flower-like cobalt particles-based magnetorheological elastomers, *Composites Communications*, vol. 15, no. July, pp. 120–128, (2019). https://doi.org/10.1016/j.coco.2019.07.007
32. Zheng, J. et al. Viscoelastic and Magnetically Aligned Flaky Fe-Based Magnetorheological Elastomer Film for Wide-Bandwidth Electromagnetic Wave Absorption, *Ind. Eng. Chem. Res.*, vol. 59, no. 8, pp. 3425–3437,https://doi.org/10.1021/acs.iecr.9b06143 (2020).
33. Yang, J., Sun, S. S., Zhang, S. W. & Li, W. H. Review of structural control technologies using magnetorheological elastomers. *Curr. Smart Mater.* **4** (1), 22–28. https://doi.org/10.2174/2405465804666190326152207 (2019).
34. Jaafar, M. F., Mustapha, F. & Mustapha, M. Review of current research progress related to magnetorheological elastomer material, https://doi.org/10.1016/j.jmrt.2021.10.058 (2021).
35. Zumelzu, E., Silva, E., Rull, F., Muñoz, O. & Ugarte, R. Effect of lactic acid on polyethylene terephthalate (PET) and polypropylene (PP) coatings of food containers. *J. Polym. Environ.* **26** (6), 2476–2488. https://doi.org/10.1007/s10924-017-1139-6 (2018).

Author contributions

Rehnupreya Hentry Viension: Writing- original draft, Methodology, Formal analysis, Conceptualization. Nur Azmah Nordin: Writing- review & editing, Validation, Supervision, Project administration, Funding acquisition, Conceptualization. Saiful Amri Mazlan: Writing- review & editing, Validation, Conceptualization. Mohd Aidy Faizal Johari: Writing- review & editing. Norman M. Wereley: Writing- review & editing. Abdul Yasser Abd Fatah: Writing- review & editing. Nursyafiqah Zaini: Writing- review & editing. Michal Sedlacik: Writing- review & editing, Funding acquisition.

Funding

This work was supported by Higher Institution Centre of Excellence (HiCOE) program of Ministry of Higher Education (MOHE) Malaysia under HiCOE Research Grant and UTM Fundamental Research (UTMFR) Grant (Q.K130000.3843.23H17). The author M.S. wishes to thank the Czech Science Foundation [25–17453 S] for the financial support.

Declarations

Competing interests

The authors declare no competing interests.

Additional information

Correspondence and requests for materials should be addressed to N.A.N. or M.S.

Reprints and permissions information is available at www.nature.com/reprints.

Publisher's note Springer Nature remains neutral with regard to jurisdictional claims in published maps and institutional affiliations.